In situ cell death detection by TUNEL assay

Endogenous peroxidase in tissue sections was blocked with 3% H_2O_2 in methanol. Sections were then incubated at 98 °C in 100 mM citrate buffer, pH 6.0, cooled, immersed in 3% normal sheep serum in TNB blocking buffer (0.1 M TRIS-HCl, pH 7.5, 0.15 M NaCl, 0.5% blocking reagent (Dupont)) and incubated at 37 °C in a TUNEL reaction mixture (Roche). After rinsing, TUNEL-positive cells were stained with converter-POD reagent and DAB substrate.

Received 6 December 2004; accepted 7 March 2005; doi:10.1038/nature03513.
Published online 27 March 2005.

1. Mowat, A. M. & Viney, J. L. The anatomical basis of intestinal immunity. *Immunol. Rev.* **156,** 145–166 (1997).
2. Veazey, R. S. *et al.* Gastrointestinal tract as a major site of $CD4^+$ T cell depletion and viral replication in SIV infection. *Science* **280,** 427–431 (1998).
3. Kewenig, S. *et al.* Rapid $CD4^+$ T cell depletion and enteropathy in simian immunodeficiency virus infected rhesus macaques. *Gastroenterology* **116,** 1115–1123 (1999).
4. Schneider, T. *et al.* Loss of CD4 T lymphocytes in patients infected with human immunodeficiency virus type 1 is more pronounced in the duodenal mucosa than in the peripheral blood. *Gut* **37,** 524–529 (1995).
5. Mehandru, S. *et al.* Primary HIV-1 infection is associated with preferential depletion of $CD4^+$ T lymphocytes from effector sites in the gastrointestinal tract. *J. Exp. Med.* **200,** 761–770 (2004).
6. Brenchley, J. M. *et al.* $CD4^+$ T cell depletion during all stages of HIV disease occurs predominantly in the gastrointestinal tract. *J. Exp. Med.* **200,** 749–759 (2004).
7. Guadalupe, M. *et al.* Severe $CD4^+$ T-cell depletion in gut lymphoid tissue during primary human immunodeficiency virus type 1 infection and substantial delay in restoration following highly active antiretroviral therapy. *J. Virol.* **77,** 11708–11717 (2003).
8. Clayton, F., Snow, G., Reka, S. & Kotler, D. P. Selective depletion of rectal lamina propria rather than lymphoid aggregate CD4 lymphocytes in HIV infection. *Clin. Exp. Immunol.* **107,** 288–292 (1997).
9. Lim, S. G. *et al.* Loss of mucosal CD4 lymphocytes is an early feature of HIV infection. *Clin. Exp. Immunol.* **92,** 448–454 (1993).
10. Veazey, R. & Lackner, A. The mucosal immune system and HIV-1 infection. *AIDS Rev.* **5,** 245–252 (2003).
11. Veazey, R. *et al.* Identifying the target cell in primary simian immunodeficiency virus infection: Highly activated memory $CD4^+$ T cells are rapidly eliminated in early SIV infection *in vivo*. *J. Virol.* **74,** 57–64 (2000).
12. Zhang, Z.-Q. *et al.* Sexual transmission and propagation of simian and human immunodeficiency viruses in two distinguishable populations of $CD4^+$ T cells. *Science* **286,** 1353–1357 (1999).
13. Zhang, Z.-Q. *et al.* Roles of substrate availability and infection of resting and activated $CD4^+$ T cells in transmission and acute simian immunodeficiency virus infection. *Proc. Natl Acad. Sci. USA* **101,** 5640–5645 (2004).
14. Boirivant, M. *et al.* HIV-1 gp120 accelerates Fas-mediated activation-induced human lamina propria T cell apoptosis. *J. Clin. Immunol.* **18,** 39–47 (1998).
15. Boirivant, M. *et al.* Stimulated human lamina propria T cells manifest enhanced Fas-mediated apoptosis. *J. Clin. Invest.* **98,** 2616–2622 (1996).
16. De Maria, R. *et al.* Functional expression of Fas and Fas ligand on human gut lamina propria T lymphocytes. A potential role for the acidic sphingomyelinase pathway in normal immunoregulation. *J. Clin. Invest.* **97,** 316–322 (1996).
17. Testi, R., Phillips, J. H. & Lanier, L. L. Constitutive expression of a phosphorylated activation antigen (Leu 23) by CD3 bright human thymocytes. *J. Immunol.* **141,** 2557–2563 (1988).
18. Testi, R., Phillips, J. H. & Lanier, L. L. Leu 23 induction as an early marker of functional CD3/T cell antigen receptor triggering. Requirement for receptor cross-linking, prolonged elevation of intracellular [Ca++] and stimulation of protein kinase C. *J. Immunol.* **142,** 1854–1860 (1989).
19. Phillips, A. N. Reduction of HIV concentration during acute infection: independence from a specific immune response. *Science* **271,** 497–499 (1996).
20. Reilly, C. S. *et al.* The clustering of SIV infected cells in lymphatic tissue. *J. Am. Stat. Assoc.* **97,** 943–954 (2002).
21. Mothe, B. R. *et al.* Dominance of CD8 responses specific for epitopes bound by a single major histocompatibility complex class I molecule during the acute phase of viral infection. *J. Virol.* **76,** 875–884 (2002).
22. Reynolds, M. R. *et al.* The $CD8^+$ lymphocyte response to major immunodominant epitopes after vaginal exposure to SIV: too late and too little. *J. Virol* (in the press).
23. Pope, M. & Haase, A. T. Transmission, acute HIV-1 infection and the quest for effective vaccines, microbicides and other strategies to prevent infection. *Nature Med.* **9,** 847–852 (2003).
24. Miller, C. J. *et al.* Intravaginal inoculation of rhesus macaques with cell-free simian immunodeficiency virus results in persistent or transient viremia. *J. Virol.* **68,** 6391–6400 (1994).
25. Poppema, S., Lai, R. & Visser, L. Monoclonal antibody OPD4 is reactive with CD45RO, but differs from UCHL1 by the absence of monocyte reactivity. *Am. J. Pathol.* **139,** 725–729 (1991).
26. Miller, C. J. *et al.* Propagation and dissemination of infection after vaginal transmission of SIV. *J. Virol* (submitted).

Acknowledgements We thank R. Veazey, L. Picker, J. Lifson, D. Douek and M. Roederer for discussions; L. Compton, D. Lu, B. Vang, K. Bost and R. Dizon of the Immunology Core Laboratory and Primate Services Unit at the CNPRC for technical assistance; and T. Leonard and C. O'Neill for help in preparing the figures and manuscript. This work was supported by grants from the National Institute of Allergy and Infectious Diseases and from the National Center for Research Resources.

Competing interests statement The authors declare that they have no competing financial interests.

Correspondence and requests for materials should be addressed to A.T.H. (haase001@umn.edu).

Clathrin is required for the function of the mitotic spindle

Stephen J. Royle[1], Nicholas A. Bright[2] & Leon Lagnado[1]

[1]*MRC Laboratory of Molecular Biology, Hills Road, Cambridge CB2 2QH, UK*
[2]*Cambridge Institute for Medical Research and Department of Clinical Biochemistry, University of Cambridge, Addenbrooke's Hospital, Hills Road, Cambridge CB2 2XY, UK*

Clathrin has an established function in the generation of vesicles that transfer membrane and proteins around the cell[1–4]. The formation of clathrin-coated vesicles occurs continuously in non-dividing cells[5], but is shut down during mitosis[6], when clathrin concentrates at the spindle apparatus[7,8]. Here, we show that clathrin stabilizes fibres of the mitotic spindle to aid congression of chromosomes. Clathrin bound to the spindle directly by the amino-terminal domain of clathrin heavy chain. Depletion of clathrin heavy chain using RNA interference prolonged mitosis; kinetochore fibres were destabilized, leading to defective congression of chromosomes to the metaphase plate and persistent activation of the spindle checkpoint. Normal mitosis was rescued by clathrin triskelia but not the N-terminal domain of clathrin heavy chain, indicating that stabilization of kinetochore fibres was dependent on the unique structure of clathrin. The importance of clathrin for normal mitosis may be relevant to understanding human cancers that involve gene fusions of clathrin heavy chain.

The subcellular distribution of clathrin depended on the phase of the cell cycle[7–9] (Supplementary Fig. 1). During interphase, green fluorescent protein (GFP)-tagged clathrin light chain a (GFP–LCa) in NRK cells was associated with the Golgi apparatus and numerous puncta representing clathrin-coated pits and vesicles[5] (Fig. 1a). But during metaphase, clathrin localized to kinetochore fibres of the mitotic spindle[10] and possibly interpolar microtubules, but not astral microtubules (Fig. 1a, b). Localization of clathrin to kinetochore fibres was confirmed by chilling cells for 10 min at 4 °C to selectively disassemble microtubules not associated with kinetochores[11]; after this treatment, clathrin in metaphase cells remained bound to the kinetochore fibres, indicating that these microtubules were a potential site of clathrin function (Fig. 1b). Similar changes in the distribution of clathrin were observed using other variants of the light chain tagged with GFP or by immunocytochemistry using a monoclonal antibody specific for clathrin heavy chain (CHC; Supplementary Figs 2 and 3).

Two observations indicated that clathrin bound to the mitotic spindle rather than membrane localized to this region. First, none of the major adaptor proteins that allow clathrin to coat membranes (AP-1, AP-2 and AP-3)[2,3] was found at the spindle apparatus (Supplementary Fig. 4a–c). To test whether clathrin at the spindle was associated with membranes at all, we indiscriminately labelled intracellular compartments by incubating cells with the styryl dye FM4-64 (15 μM) for >24 h (Supplementary Fig. S4d). In cells at metaphase, none of these membranes was found at the spindle (Fig. 1c).

The localization of clathrin to the mitotic spindle was examined at higher resolution using immunoelectron microscopy. CHC and α-tubulin were immunolabelled with 15-nm and 10-nm colloidal-gold-conjugated reagents, respectively (Fig. 1d). CHC in mitotic NRK cells was associated with electron-dense tracks that were directed towards the chromosomes, and these tracks were confirmed as microtubules by labelling for α-tubulin (Fig. 1d, top left and right panels). Clathrin-coated vesicles were scarce in mitotic cells but when visualized (Fig. 1d, bottom left panel) they could be distinguished from microtubule-associated clathrin (Fig. 1d, right

panel). Furthermore, clathrin immunoreactivity persisted at the spindle after soluble proteins had been removed from cells by detergent extraction (Supplementary Fig. 3). Together, these results indicated that clathrin at the mitotic spindle was not coating membranes but was bound to microtubules or microtubule-associated protein(s). Direct binding of CHC to the spindle apparatus has also been demonstrated by mass spectrometry[12].

To identify the region of clathrin that determined its association with the mitotic spindle, recruitment was quantified using a simple assay that compared the intensity of fluorescent proteins in the region of the spindle relative to the cytoplasm (see Methods). GFP–LCa was recruited to the spindle when CHC was abundant in cells, but not when CHC was depleted by RNA interference (RNAi), indicating that the determinant for spindle binding was contained in the heavy chain (Fig. 2a, b). To localize the region further, GFP-tagged fragments of CHC were expressed and their recruitment to the spindle quantified (Fig. 2c–e). CHC fragments containing the N-terminal domain (GFP–CHC(1–1074) and GFP–CHC(1–479)) and the N-terminal domain itself (GFP–CHC(1–330)) were recruited, but a long construct lacking this region (GFP–CHC(331–1074)) was not (Fig. 2d, e). These results indicate that clathrin triskelia bound to the mitotic spindle via the N-terminal domain of the heavy chain.

Having characterized how clathrin becomes associated with the mitotic spindle, we went on to investigate whether it had any role in mitosis by using RNAi to deplete rat or human cells of CHC (see Supplementary Information). In NRK cells 72 h after transfection, the level of CHC at interphase was ~10% of controls and clathrin-mediated endocytosis was reduced by more than 90% (Supplementary Fig. 5). At metaphase, the level of CHC at the spindle was 11 ± 2% of control levels 72 h after transfection with short interfering (si)RNA. RNAi-mediated depletion of CHC also reduced proliferation of cells twofold, even though the proportion of dead or dying cells was only ~0.3%, as judged by nuclear morphology[13,14].

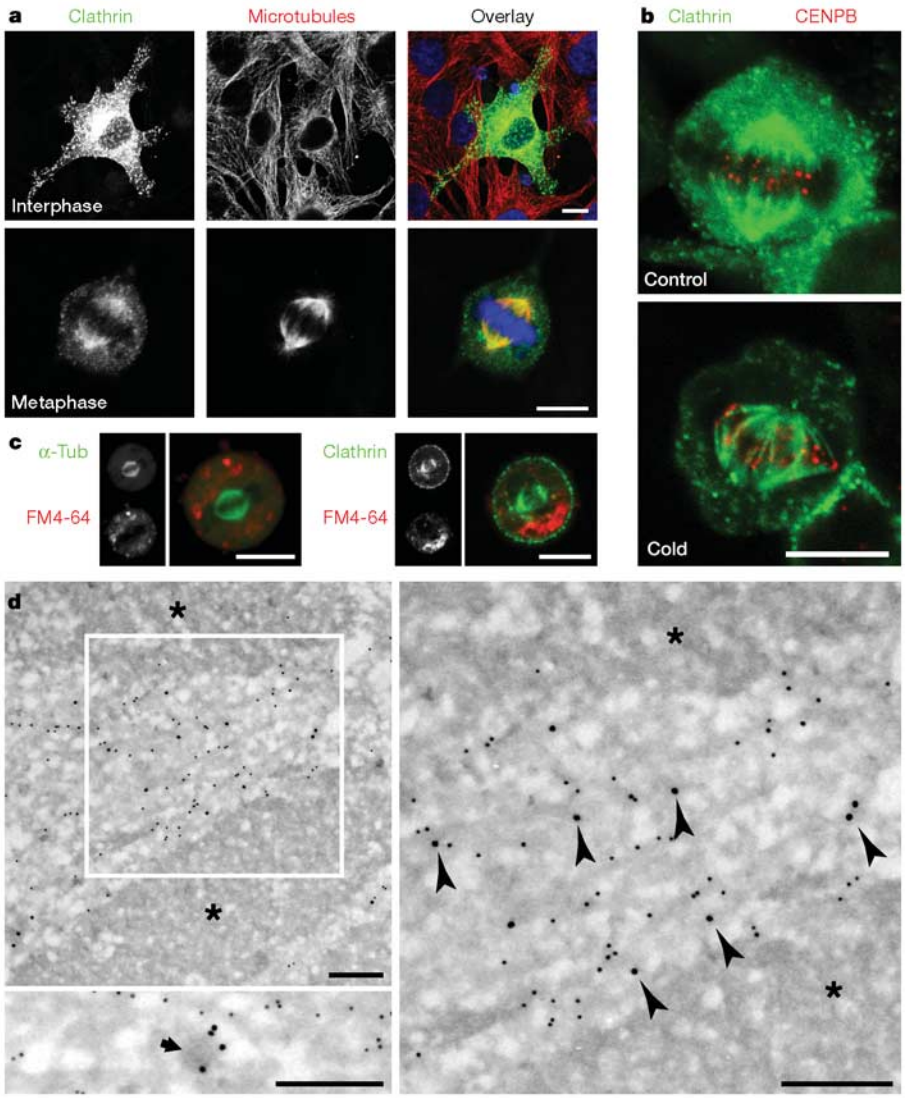

Figure 1 Clathrin was targeted to the mitotic spindle of NRK cells. **a**, Confocal micrographs showing the subcellular distribution of clathrin at interphase and metaphase. GFP–LCa (left, green), α-tubulin (centre, red) and nucleic acid (blue) staining is shown. **b**, Cells expressing GFP–LCa fixed before (top) or after (bottom) cold treatment to depolymerize non-kinetochore microtubules. CENPB, centromere protein B. **c**, **d**, The association of clathrin with microtubules is not via coated membranes. **c**, Example images of live cells expressing either GFP–α-tubulin (left) or GFP–LCa (right) imaged after 24–28-h incubation with FM4-64 (red). **d**, Association of clathrin with microtubules visualized by immunogold electron microscopy. CHC (15 nm gold) and α-tubulin (10 nm gold) in mitotic NRK cells. Chromosomes are denoted by asterisks. A morphologically distinct clathrin-coated vesicle (bottom left panel) is indicated by an arrow. Arrowheads denote CHC labelling associated with microtubules. Scale bars: 10 μm (**a**–**c**); 250 nm (**d**).

Reduced proliferation was associated with prolonged mitosis, because the proportion of cells in mitosis (the mitotic index) was increased fourfold 72 h after CHC RNAi transfection (rat: control 3.5 ± 0.2%, knockdown 14.2 ± 1.1% (Fig. 3a); human: control 1.9 ± 0.21%, knockdown 8.4 ± 0.6; $P < 0.001$; data not shown).

Does prolonged mitosis in cells depleted of CHC represent an alternative function of clathrin or an indirect effect of inhibiting clathrin-mediated endocytosis? To investigate this question a dominant-negative inhibitor of clathrin-mediated endocytosis was used as an alternative method of inhibiting the established function of clathrin. When GFP–CHC(1–479) was overexpressed in NRK cells, uptake of fluorescent transferrin was inhibited by 60–70% during a 48–96 h period after transfection, but the mitotic index was not affected (Fig. 3b). Overexpression of GFP–CHC(1–479) inhibited clathrin-mediated endocytosis without significantly affecting the binding of clathrin to the spindle: spindles in GFP–CHC(1–479)-expressing cells had 94 ± 6% of the clathrin immunoreactivity observed in cells expressing GFP alone. The prolongation of mitosis in cells depleted of clathrin therefore reflected a direct action of clathrin at the mitotic spindle, distinct from its role in membrane transport. This conclusion was reinforced by two observations. First, clathrin-mediated endocytosis was shut down during mitosis (transferrin uptake in mitotic cells was 10 ± 6% of that at interphase)[6]. Second, knockdown of CHC caused a series of mitotic defects (described below), none of which was observed in cells in which clathrin-mediated endocytosis was inhibited by expression of GFP–CHC(1–479).

A number of observations indicated that clathrin regulated the congression of chromosomes. First, when we examined the proportion of cells at each stage of mitosis, more were in prometaphase after clathrin knockdown compared with controls (49 ± 6% versus 31 ± 6%, $P < 0.05$; Supplementary Fig. 5f). Second, the metaphase plate was thicker in clathrin-depleted cells (11.2 ± 0.9 μm compared with 7.0 ± 0.5 μm in controls; Fig. 4a) and centromeres did not organize on the mitotic spindle in an orderly manner (Fig. 4b). Third, there was an increased incidence of misaligned chromosomes

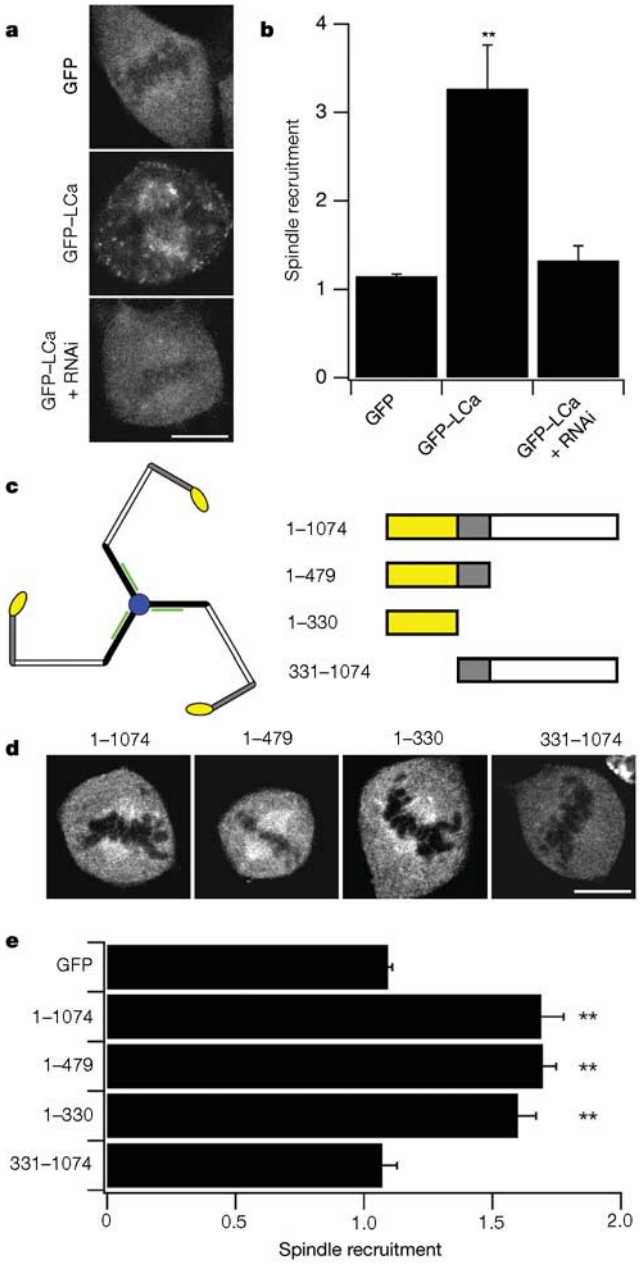

Figure 2 Clathrin was targeted to the mitotic spindle via the N-terminal domain of the heavy chain. **a**, Example images of GFP and GFP–LCa in cells at metaphase. **b**, Histogram of spindle recruitment of GFP or GFP–LCa. A value of one represents no specific recruitment (see Methods). **c**, Schematic diagram of a clathrin triskelion and the CHC fragments used in **d**, **e**. The CHC N-terminal domain forming the 'foot' is yellow (residues 1–330). **d**, Example images of GFP-tagged CHC fragments in cells at metaphase. **e**, Histogram of spindle recruitment of GFP or GFP-tagged CHC fragments. Results are mean ± s.e.m.; double asterisk, $P < 0.01$. Scale bars: 10 μm.

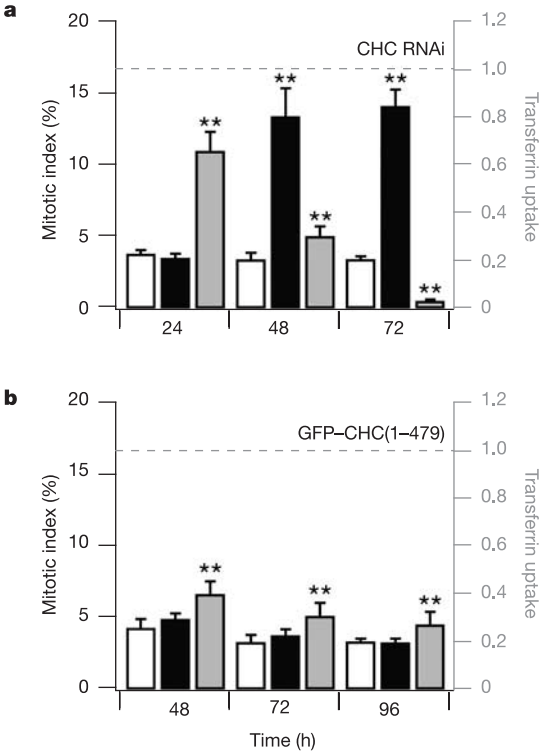

Figure 3 Inhibition of clathrin-mediated endocytosis did not disrupt mitosis. **a**, Effect of clathrin depletion on mitotic index (black bars) and transferrin uptake (grey bars) 24, 48 and 72 h after transfection with CHC siRNA. Open bars show mitotic index in control siRNA-transfected cells. Transferrin uptake was normalized to control values (dotted line). Within 48 h clathrin-mediated endocytosis was reduced by 70% and the mitotic index increased fourfold. **b**, Effects of inhibiting clathrin-mediated endocytosis by overexpression of GFP–CHC(1–479), measured 48, 72 and 96 h after transfection. Transferrin uptake was inhibited by 60–70%, without any change in the mitotic index. Control (open bars) was GFP alone. Results are mean ± s.e.m.; double asterisk, $P < 0.01$.

in metaphase-like cells after clathrin knockdown (Fig. 4a; see also the right CHC RNAi panel of c and e for other examples). Misaligned chromosomes were normally observed in 4 ± 1% of rat cells at metaphase and 10 ± 7% of human cells. However, after depletion of clathrin, misaligned chromosomes were observed in 22 ± 5% of rat cells and 70 ± 7% of human cells that appeared to be in metaphase. In these human cells, there was an average of 3.4 ± 0.8 misaligned chromosomes per cell. Misaligned chromosomes were usually found at spindle poles; they always consisted of pairs of sister chromatids (Fig. 4d) but they did not have spindle attachments (Fig. 4c, right CHC RNAi panel) and the arms were very rarely in the V-shaped configuration typical of congressing chromosomes[15]. Misaligned chromosomes therefore arose owing to a failure in congression during prometaphase rather than premature separation of sister chromatids.

Kinetochore fibres exert tension on sister chromatids that can be assessed by measuring the interkinetochore distance[16]. At early prometaphase, before chromosomes attach to the spindle, this distance was 0.8 ± 0.02 μm in controls and 0.8 ± 0.02 μm in cells depleted of clathrin. The upper 95% confidence interval of the control distribution was 1.2 μm, so interkinetochore distances greater than this threshold value could be taken as evidence that the sister chromatids were under tension. Misaligned chromosomes in clathrin-depleted cells at metaphase were not under tension, because the interkinetochore distance averaged 0.9 ± 0.05 μm ($P = 0.151$). At metaphase, the interkinetochore distance of equatorial chromosomes averaged 1.6 ± 0.04 μm in control cells, but was significantly less in cells depleted of clathrin (1.3 ± 0.03 μm; $P < 0.01$). Notably, only 2% of kinetochore pairs were at a distance less than 1.2 μm at the metaphase plate of control cells, but this reached 20% in cells depleted of clathrin. These results indicate that clathrin knockdown led to a reduction in tension exerted on sister chromatids of some chromosomes. Clathrin knockdown also reduced the stability of kinetochore–spindle contacts. In control cells at metaphase, all kinetochores had an attached fibre, as judged by the selective depolymerization of microtubules not attached to kinetochores (Fig. 4c). In contrast, clathrin-depleted cells often contained 'orphan' centromeres that did not have a fibre attached (Fig. 4c, left CHC RNAi panel), suggesting that congression had occurred but that the fibre had been lost subsequently.

The transition from metaphase to anaphase is controlled by the spindle checkpoint, which monitors correct attachment of chromosomes to kinetochore fibres[17]. Persistent activation of the checkpoint prolongs mitosis[17]. One component of the checkpoint is Mad2, which we visualized by coupling expression of GFP–hMad2 (ref. 18) to either control or CHC short hairpin RNA (shRNA) in human cells using pBrain vectors (see Methods). In cells co-expressing control shRNA, GFP–hMad2 correctly localized to kinetochores in early prometaphase (not shown) and then became diffusely distributed at metaphase[18] (Fig. 4e, left panel).

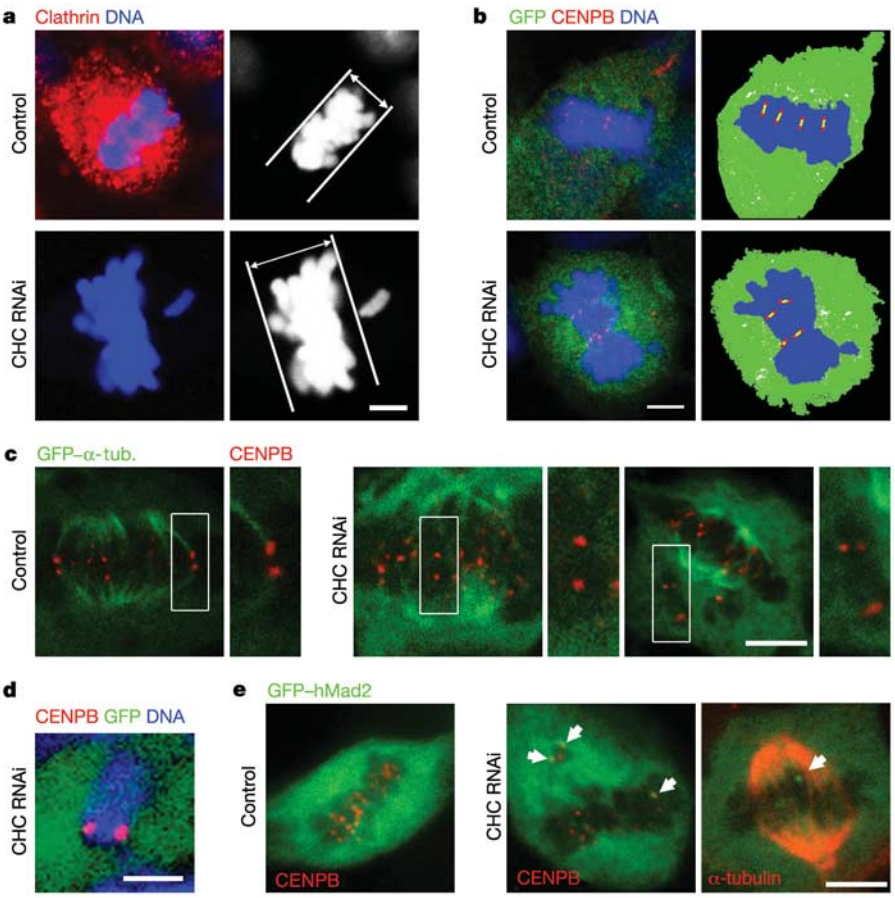

Figure 4 Depletion of clathrin results in destabilized kinetochore fibres, defective congression of chromosomes and prolonged activation of the spindle checkpoint. **a**, Clathrin depletion increased the frequency of misaligned chromosomes and caused thicker metaphase plates (parallel lines). **b**, Clathrin-depleted metaphase-like plates were disorganized. Cells were marked by GFP (green) and stained for nucleic acids (blue) and CENPB (red) to visualize centromeres. Schematic drawings illustrate centromere arrangement (right). **c**, Cells expressing GFP–α-tubulin (green) after depolymerization of non-kinetochore fibres. The right panels show a higher magnification of boxed centromere pairs. **d**, Misaligned chromosomes in CHC RNAi cells were pairs of sister chromatids. **e**, Representative images of one control (left) and two CHC RNAi (middle and right panels) cells expressing very low levels of GFP–hMad2. Mad2-positive kinetochores are indicated by arrows. Scale bars: 5 μm.

But in cells co-expressing CHC shRNA, Mad2 signalling persisted during metaphase: GFP–hMad2 was found on the kinetochores of misaligned chromosomes as well as chromosomes at the metaphase plate (Fig. 4e). Staining for α-tubulin revealed that Mad2-positive kinetochores had no obvious microtubular connections (Fig. 4e, right panel). Similar observations were made using anti-Mad2 (Supplementary Fig. 7b, c). These results indicate that the primary cause of prolonged mitosis in cells depleted of clathrin was the continued activation of the spindle checkpoint, which resulted from destabilization of kinetochore microtubules.

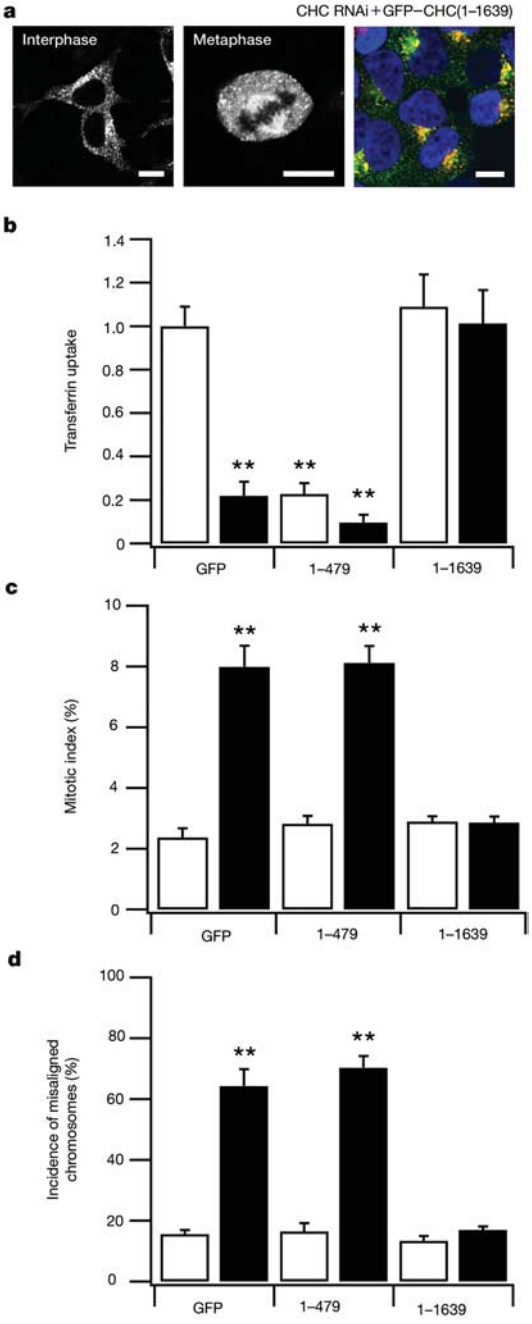

Figure 5 Full-length CHC, but not CHC N-terminal domain, is sufficient to rescue the mitotic defects found in cells depleted of endogenous CHC. **a**, Representative images of GFP-tagged knockdown-resistant CHC (GFP-CHC(1-1639)) expressed in HEK293 cells that were depleted of endogenous CHC. The right panel shows the normal uptake of transferrin (red), GFP–CHC(1–1639) (green) and DNA (blue) in these cells. **b**–**d**, Quantification of transferrin uptake at interphase (**b**), mitotic index (**c**) and the frequency of metaphase-like cells with misaligned chromosomes (**d**) in cells expressing GFP, GFP–CHC(1-479) or GFP-CHC(1–1639) 72 h after transfection. Open bars, control cells; filled bars, cells depleted of endogenous CHC. Results are mean ± s.e.m.; double asterisk, $P < 0.01$.

How might clathrin influence the stability of kinetochore fibres? Free clathrin occurs as triskelia[4,19], and the N-terminal domain at the foot of each leg, which is required for binding to the spindle (Fig. 2), also interacts with a large number of proteins[20,21]. One possibility is that clathrin triskelia stabilize kinetochore fibres by acting as a brace connecting two or three microtubules within a fibre. Alternatively, the N-terminal domain might simply recruit another protein required for stabilization of spindle fibres. To distinguish between these two possibilities, we tested whether clathrin triskelia or the N-terminal domain alone could rescue the mitotic defects in cells depleted of endogenous clathrin. For these experiments we expressed either GFP (control), GFP–CHC(1–479) or full-length GFP–CHC(1–1639) in control or CHC RNAi cells, while making the CHC components resistant to RNAi by silent mutations in the shRNA-binding region (see Methods). For full-length CHC we used the major human splice variant that encodes residues 1–1639. Two observations indicated that GFP–CHC(1–1639) formed triskelia with normal function in clathrin-mediated endocytosis. First, this construct labelled punctate structures in interphase cells and decorated the mitotic spindle at metaphase (Fig. 5a), similar to GFP–LCa[5] (Fig. 1). Second, GFP–CHC(1–1639) supported the uptake of transferrin in a manner indistinguishable from wild-type CHC (Fig. 5a, b). GFP–CHC(1–1639) also corrected mitotic defects in cells depleted of endogenous clathrin, preventing the prolongation of mitosis (Fig. 5c) and returning the incidence of misaligned chromosomes to normal levels (Fig. 5d). In contrast, the N-terminal domain alone had no significant effect on mitigating these consequences of clathrin knockdown (Fig. 5c, d). We conclude that stabilization of kinetochore fibres requires the trimeric structure of clathrin rather than the interaction function of the N-terminal domain.

Kinetochore fibres might be strengthened if clathrin triskelia form a relatively rigid connection between microtubules. In agreement with this idea, electron micrographs show that microtubules within the spindle fibres are connected by curved 'bridges'[10,22], the molecular identities of which are currently unknown. These bridges result in 50–100-nm spacing between microtubules in spindle fibres[10]. By comparison, the distance between N-terminal domains of free triskelia is 45–70 nm[19,23].

We found an increased frequency of misaligned chromosomes in cells depleted of clathrin (Figs 4 and 5). The mis-segregation of chromosomes during mitosis is a potential source of aneuploidy, a form of genetic instability that may lead to cancer or birth defects[24]. Given the evidence that clathrin has an alternative function in mitosis, it may be worth re-assessing the involvement of gene fusions of CHC with anaplastic lymphoma kinase (ALK)[25] in inflammatory myofibroblastic tumours and anaplastic large-cell lymphoma, as well as the fusion of CHC with the transcription factor gene *TFE3* in renal adenocarcinomas[26]. These gene fusions occur at the carboxy-terminal end of CHC, and are therefore expected to disrupt trimerization while allowing binding to the mitotic spindle. On the basis of our results, we suggest that these fusion proteins might impair the function of clathrin during mitosis, or in the case of CHC–ALK, target a catalytically active fragment of ALK to the mitotic spindle.

The role of clathrin in the transport of membrane and proteins has been studied intensively[1–3]. Here, we have provided evidence for a second important function of clathrin, which occurs during mitosis; that is, the stabilization of kinetochore fibres of the spindle apparatus. Future studies will seek to identify protein partners for clathrin at the spindle and understand how clathrin switches between its two functions. □

Methods

Molecular biology

GFP–LCa was generated by polymerase chain reaction to introduce *Bgl*II and *Eco*RI sites, and subcloned into pEGFP-C1 (Clontech). GFP–CHC(1–479), GFP–CHC(1–330) and GFP–CHC(331–1074) were amplified and subcloned into *Bgl*II and *Hin*dIII sites of pEGFP-C1, and GFP–CHC(1–1074) was made by subcloning a *Bgl*II–*Sca*I fragment from GFP–CHC(1–479) into GFP–CHC(331–1074). GFP–hMad2 was reconstructed to enable us to make pBrain versions (see below). GFP–hMad2 in pCS2 was amplified to introduce *Bgl*II and *Hin*dIII sites, and the resulting fragment was cloned into pEGFP-C1. Human CHC and clathrin light chain LCa complementary DNAs (I.M.A.G.E. 6187185 and 3944942) were purchased from MRC Geneservice. GFP-tagged α-tubulin was from Clontech (pEGFP-Tub). GFP–hMad2 in pCS2 (ref. 18) was a gift from G. Fang. A series of vectors (pBrain) were made that allowed the simultaneous expression of shRNA under an H1 RNA promoter and fluorescent proteins under a CMV promoter. For rescue experiments, GFP–CHC(1–479) was rendered resistant to knockdown ('knockdown-proof'; KDP) by mutation using the megaprimer method to give GFP–CHC(1–479)KDP. Knockdown-proof GFP–CHC(1–1639) was made by subcloning an *Age*I–*Mfe*I fragment into pEGFP-C1 at *Xma*I–*Mfe*I sites and then repairing the N terminus by substituting a *Bgl*II–*Asp*718 fragment from GFP–CHC(1–479)KDP. All constructs used in this study were verified by automated DNA sequencing (Lark or MRC Geneservice).

Immunocytochemistry

Immunostaining was performed as described previously[27]. The following monoclonal antibodies were used: anti-clathrin heavy chain and anti-α-adaptin (X22 and AP6, Affinity BioReagents); anti-α-tubulin and anti-β1/2-adaptin (DM1A and 100/1, Sigma); anti-CENPB (a gift from W. C. Earnshaw); and anti-δ-adaptin (clone SA4; a gift from M. S. Robinson). Rabbit polyclonal anti-clathrin antiserum was as previously described[28]. Goat anti-mouse or anti-rabbit Cy3-conjugated secondary antibodies were from Jackson ImmunoResearch. Goat anti-mouse IgG conjugated to 10-nm colloidal gold was from Biocell. Protein A conjugated to 15-nm colloidal gold was from the Department of Cell Biology, University of Utrecht. TOPRO-3 (Molecular Probes) and Hoechst 33342 (Sigma) were used for staining DNA/RNA. Uptake of transferrin-Alexa546 (Molecular Probes) was done as previously described[29]. FM4-64 was from Calbiochem. For membrane-labelling experiments, transfected cells were cultured for >24 h in 15 μM FM4-64 at 37 °C, and cells were washed for 5 min in imaging buffer (MEM without phenol red, 10% FBS, 100 U ml^{-1} penicillin/streptomycin) before images were taken.

Imaging

Confocal imaging was done using a BioRad Radiance 2000 and Nikon TE300 microscope with × 60 (1.4 NA) or × 100 (1.3 NA) oil immersion objectives. GFP, Cy3 or FM4-64, and TOPRO-3 were excited at 488, 543 and 633 nm, respectively. For quantitative immunostaining experiments, identical laser power and acquisition settings were used. Images (8-bit) were imported into IMAGEJ (NIH) or IPLab 3.9 (Scanalytics). To quantify the uptake of transferrin-Alexa546, the outline of the cell was drawn on the GFP channel of the image and this region of interest (ROI) was transferred to the red channel, the image was assigned a threshold and the number of transferrin puncta counted. Spindle recruitment was assayed by dividing the mean pixel density measured in a 1 × 1 μm ROI placed over the spindle by that measured in a region outside the spindle.

The mitotic index was determined by counting the number of cells in mitosis as a proportion of the total number of cells within a 275 × 190 μm area. For image quantification and counting experiments, between 5–80 cells were analysed and 100–3,914 cells were counted from experiments performed three to six times. Results are expressed as mean ± s.e.m.; unpaired Student's *t*-test was used to compare control and test values, and analysis of variance (ANOVA) with Dunnet's post-hoc test was used to compare multiple groups to a control. For binomial results (mitotic index, misaligned chromosomes, multinucleate cells, and so on) data were tested for approximation to a normal distribution, *z*-values were calculated and *P*-values were retrieved using Microsoft Excel.

Immunoelectron microscopy

Cells were prepared for ultra-structural analysis using immunogold electron microscopy as previously described[30]. Briefly, mitotic NRK cells were fixed with 4% paraformaldehyde/0.1% glutaraldehyde in 0.1 M sodium cacodylate, pH 7.2 at room temperature for 1 h, infused with 1.7 M sucrose/15% polyvinylpyrolidone and prepared as previously described[30]. Ultra-thin frozen sections were collected from the knife edge with 50:50 2% methyl cellulose:2.3 M sucrose and immunolabelled, contrasted with methyl cellulose/uranyl acetate, dried and observed in a Philips CM100 TEM[30]. (See Supplementary Information for a complete description of the Methods.)

Received 7 January; accepted 1 March 2005; doi:10.1038/nature03502.

1. Kirchhausen, T. Clathrin. *Annu. Rev. Biochem.* **69,** 699–727 (2000).
2. Brodsky, F. M., Chen, C. Y., Knuehl, C., Towler, M. C. & Wakeham, D. E. Biological basket weaving: formation and function of clathrin-coated vesicles. *Annu. Rev. Cell Dev. Biol.* **17,** 517–568 (2001).
3. Robinson, M. S. Adaptable adaptors for coated vesicles. *Trends Cell Biol.* **14,** 167–174 (2004).
4. Fotin, A. *et al.* Molecular model for a complete clathrin lattice from electron cryomicroscopy. *Nature* **432,** 573–579 (2004).
5. Gaidarov, I., Santini, F., Warren, R. A. & Keen, J. H. Spatial control of coated-pit dynamics in living cells. *Nature Cell Biol.* **1,** 1–7 (1999).
6. Warren, G. Membrane partitioning during cell division. *Annu. Rev. Biochem.* **62,** 323–348 (1993).
7. Maro, B., Johnson, M. H., Pickering, S. J. & Louvard, D. Changes in the distribution of membranous organelles during mouse early development. *J. Embryol. Exp. Morphol.* **90,** 287–309 (1985).
8. Okamoto, C. T., McKinney, J. & Jeng, Y. Y. Clathrin in mitotic spindles. *Am. J. Physiol. Cell Physiol.* **279,** C369–C374 (2000).
9. Sutherland, H. G. *et al.* Large-scale identification of mammalian proteins localized to nuclear sub-compartments. *Hum. Mol. Genet.* **10,** 1995–2011 (2001).
10. Compton, D. A. Spindle assembly in animal cells. *Annu. Rev. Biochem.* **69,** 95–114 (2000).
11. Yao, X., Abrieu, A., Zheng, Y., Sullivan, K. F. & Cleveland, D. W. CENP-E forms a link between attachment of spindle microtubules to kinetochores and the mitotic checkpoint. *Nature Cell Biol.* **2,** 484–491 (2000).
12. Mack, G. J. & Compton, D. A. Analysis of mitotic microtubule-associated proteins using mass spectrometry identifies astrin, a spindle-associated protein. *Proc. Natl Acad. Sci. USA* **98,** 14434–14439 (2001).
13. Motley, A., Bright, N. A., Seaman, M. N. & Robinson, M. S. Clathrin-mediated endocytosis in AP-2-depleted cells. *J. Cell Biol.* **162,** 909–918 (2003).
14. Hinrichsen, L., Harborth, J., Andrees, L., Weber, K. & Ungewickell, E. J. Effect of clathrin heavy chain- and α-adaptin-specific small inhibitory RNAs on endocytic accessory proteins and receptor trafficking in HeLa cells. *J. Biol. Chem.* **278,** 45160–45170 (2003).
15. Skibbens, R. V., Skeen, V. P. & Salmon, E. D. Directional instability of kinetochore motility during chromosome congression and segregation in mitotic newt lung cells: a push-pull mechanism. *J. Cell Biol.* **122,** 859–875 (1993).
16. Waters, J. C., Skibbens, R. V. & Salmon, E. D. Oscillating mitotic newt lung cell kinetochores are, on average, under tension and rarely push. *J. Cell Sci.* **109,** 2823–2831 (1996).
17. Cleveland, D. W., Mao, Y. & Sullivan, K. F. Centromeres and kinetochores: from epigenetics to mitotic checkpoint signaling. *Cell* **112,** 407–421 (2003).
18. Howell, B. J., Hoffman, D. B., Fang, G., Murray, A. W. & Salmon, E. D. Visualization of Mad2 dynamics at kinetochores, along spindle fibers, and at spindle poles in living cells. *J. Cell Biol.* **150,** 1233–1250 (2000).
19. Ungewickell, E. & Branton, D. Assembly units of clathrin coats. *Nature* **289,** 420–422 (1981).
20. ter Haar, E., Harrison, S. C. & Kirchhausen, T. Peptide-in-groove interactions link target proteins to the β-propeller of clathrin. *Proc. Natl Acad. Sci. USA* **97,** 1096–1100 (2000).
21. Miele, A. E., Watson, P. J., Evans, P. R., Traub, L. M. & Owen, D. J. Two distinct interaction motifs in amphiphysin bind two independent sites on the clathrin terminal domain β-propeller. *Nature Struct. Mol. Biol.* **11,** 242–248 (2004).
22. Hepler, P. K., McIntosh, J. R. & Cleland, S. Intermicrotubule bridges in mitotic spindle apparatus. *J. Cell Biol.* **45,** 438–444 (1970).
23. Kirchhausen, T., Harrison, S. C. & Heuser, J. Configuration of clathrin trimers: evidence from electron microscopy. *J. Ultrastruct. Mol. Struct. Res.* **94,** 199–208 (1986).
24. Jallepalli, P. V. & Lengauer, C. Chromosome segregation and cancer: cutting through the mystery. *Nature Rev. Cancer* **1,** 109–117 (2001).
25. Pulford, K., Morris, S. W. & Turturro, F. Anaplastic lymphoma kinase proteins in growth control and cancer. *J. Cell. Physiol.* **199,** 330–358 (2004).
26. Argani, P. *et al.* A novel CLTC-TFE3 gene fusion in pediatric renal adenocarcinoma with t(X;17)(p11.2;q23). *Oncogene* **22,** 5374–5378 (2003).
27. Bobanovic, L. K., Royle, S. J. & Murrell-Lagnado, R. D. P2X receptor trafficking in neurons is subunit specific. *J. Neurosci.* **22,** 4814–4824 (2002).
28. Simpson, F. *et al.* A novel adaptor-related protein complex. *J. Cell Biol.* **133,** 749–760 (1996).
29. Royle, S. J., Bobanovic, L. K. & Murrell-Lagnado, R. D. Identification of a non-canonical tyrosine-based endocytic motif in an ionotropic receptor. *J. Biol. Chem.* **277,** 35378–35385 (2002).
30. Bright, N. A., Reaves, B. J., Mullock, B. M. & Luzio, J. P. Dense core lysosomes can fuse with late endosomes and are re-formed from the resultant hybrid organelles. *J. Cell Sci.* **110,** 2027–2040 (1997).

Supplementary Information accompanies the paper on **www.nature.com/nature**.

Acknowledgements We thank W. C. Earnshaw, G. Fang, G. Ihrke, A. P. Jackson and M. S. Robinson for their gifts of antibodies, plasmids and cells. We also thank J. W. Raff and M. S. Robinson for useful discussion. This work was supported by the MRC and the Human Frontiers Science Program (grant to L.L.). N.A.B. was funded by the MRC.

Competing interests statement The authors declare that they have no competing financial interests.

Correspondence and requests for materials should be addressed to S.J.R. (sjr51@mrc-lmb.cam.ac.uk).